PHYSICAL REVIEW D **86,** 074512 (2012)

Quark flavor effects on gluon and ghost propagators

A. Ayala,[1] A. Bashir,[2,3,4] D. Binosi,[5] M. Cristoforetti,[5,6] and J. Rodríguez-Quintero[1]

[1]*Departamento Física Aplicada, Facultad Ciencias Experimentales, Universidad de Huelva, 21071 Huelva, Spain*
[2]*Instituto de Física y Matemática, Universidad Michoacana de San Nicolás de Hidalgo, Edificio C-3, Ciudad Universitaria, Morelia, Michoacán 58040, Mexico*
[3]*Physics Division, Argonne National Laboratory, Argonne, Illinois 60439, USA*
[4]*Center for Nuclear Research, Department of Physics, Kent State University, Kent, Ohio 44242, USA*
[5]*European Center for Theoretical Studies in Nuclear Physics and Related Areas (ECT*) and Fondazione Bruno Kessler, Villa Tambosi, Strada delle Tabarelle 286, I-32123 Villazzano (TN), Italy*
[6]*LISC, Via Sommarive 18, Povo (Trento), I-38123 Italy*

(Received 5 August 2012; published 17 October 2012)

We compute the full nonperturbative ghost and gluon two-point Green functions by using gauge field configurations with $N_f = 2$ and $N_f = 2 + 1 + 1$ twisted-mass quark flavors. We use simulations with several different light quark masses, heavy quark masses close to that of the strange and charm quarks, and the lightest pseudoscalar masses ranging from 270 to 510 [MeV]. Quark flavor effects on both the gluon and the ghost propagators are then investigated in a wide range of momenta, bridging the deep infrared and intermediate momenta domain of QCD interactions in the presence of dynamical quarks. The ghost-gluon vertex is also indirectly probed through a consistency requirement among the lattice data for the gluon and ghost propagators and the ghost propagator Schwinger-Dyson equation. The effective full QCD coupling is finally constructed, and its dependence on the presence of dynamical fermions scrutinized.

DOI: 10.1103/PhysRevD.86.074512 PACS numbers: 11.15.Ha, 11.15.Tk, 12.38.Aw, 12.38.Gc

I. INTRODUCTION

During the past few years, lattice simulations have considerably improved our understanding of the infrared (IR) sector of non-Abelian Yang-Mills theories. In particular, *quenched* Landau gauge simulations [1,2], performed on lattices with large volumes, have unequivocally demonstrated that the gluon propagator saturates in the (deep) IR region. This is true for the space-time dimensions $d = 3$ as well as 4, irrespectively of the number of colors N_C of the gauge group $SU(N_C)$ under consideration. At the same time, the ghost dressing function effectively acquires its tree-level behavior, with the functional form of the propagator being $\sim 1/q^2$.

Within the continuum formulation of the theory, these lattice results are in agreement with the solutions of the corresponding all-order Schwinger-Dyson equations (SDEs) [3,4] and exact renormalization group (RG) equations [5]. Other approaches such as the so-called refined Gribov-Zwanziger formalism [6] also converge to the same conclusions. This has caused a paradigmatic shift among practitioners: the gluon is now thought to acquire a momentum-dependent mass $m(q^2)$ whose magnitude can be large at IR momenta, but vanishes with increasing spacelike momenta (i.e., $q^2 \gg \Lambda^2_{\rm QCD}$), thereby maintaining full accord with perturbative QCD. Gluon confinement is then realized, as it is customarily done in the case of quarks, through the violation of reflection positivity (signaled by the presence of an inflection point of the propagator scalar cofactor $\Delta(q^2)$) instead of achieving an area law for a Wilson loop or a linearly rising potential (criteria which are irrelevant to the question of light-quark confinement [7]), or satisfying *ad hoc* criteria involving the ghost sector (which, as already pointed out above, completely decouples in this regime).

The extension of these quenched lattice results to full QCD, i.e., to a non-Abelian $SU(3)$ theory with the inclusion of dynamical quarks, has not been extensively pursued, neither in the continuum nor on the lattice. In the former case, an analysis of the effects on the gluon propagator due to dynamical quarks has recently been reported in Ref. [8] within the so-called pinch technique-background field method (PT-BFM) truncation scheme [9] (for a similar analysis in the context of the IR divergent 'scaling' solutions see Ref. [10]). Earlier related endeavours on the lattice can be traced back to Ref. [11] where an $\mathcal{O}(a^2)$ Symanzik-improved action with $2 + 1$ staggered fermion flavors was employed, and Ref. [12] where a tadpole-improved gauge action with two dynamical overlap fermions was used instead. However, an independent affirmation of these results by implementing different lattice actions[1] as well as their extension for different numbers of flavors, has been a pending issue since then.

This article provides a comprehensive quantitative study of the aforementioned Green functions which incorporate the effects stemming from the presence of dynamical quarks. To this end, we compute the gluon and ghost two-point Green functions from the gauge configurations generated by the ETM collaboration [14,15] for the cases

[1]Some preliminary results obtained from simulations with large lattice sizes (far from the continuum limit) and $N_f = 2$ Wilson-Clover fermions have also been reported in Ref. [13].

of (i) two light degenerate quarks ($N_f = 2$) and (ii) two light and two heavy[2] ($N_f = 2 + 1 + 1$) mass-twisted lattice flavors [16]. Furthermore, we apply our lattice results to carry out an indirect study of the ghost-gluon form factor (as done for quenched lattice data in Ref. [17]), by employing a hybrid approach where the solutions of the ghost SDE are studied using the gluon propagator determined in our simulations as an input. Consequently, the natural requirement to reproduce the lattice ghost dressing function data from the corresponding SDE solution will pin down the ghost-gluon vertex form factor, which will be shown to deviate considerably from its tree-level value. The constructed SDE solutions then allow us to extrapolate the lattice ghost data down to the vanishing momentum region and obtain reliable information on the saturation point of both the ghost dressing function as well as of the so-called Kugo-Ojima parameter [18]. Finally, the QCD effective charge, defined in Ref. [19], is computed by properly combining the gluon propagator and the ghost dressing function with the lattice estimate of the coupling in the so-called Taylor scheme (e.g., see Ref. [20]) at a given (large enough) momentum.

The main results of this article can be summarized as follows.

(i) The effect of the presence of dynamical quarks on the gluon propagator Δ is twofold: a suppression of both the *swelling* region at intermediate momenta and the saturation value in the deep IR (which can be interpreted as the gluon becoming more massive in the presence of quarks). In addition, one observes that the more light flavors there are, the bigger the effect is, which is in accordance with what we would naturally expect. Light virtual quarks can be copiously produced, thus screening the interaction and suppressing the very same mechanism which triggers gluon mass generation. As the fermion mass is increased (at a fixed flavor number) the effect gets smaller, since the heavier the fermions, the lesser is the statistical likelihood of their pair production. At a sufficiently large value of their mass, they essentially decouple and the gluon mass generation is practically insensitive to their presence. With respect to this point it should be noticed that our results turn out to be in agreement with the SDE study reported in Ref. [8] confirming at the same time the general trend reported in the earlier lattice studies of Refs. [11–13].

(ii) On the other hand, the effect on the ghost dressing function F is much milder and is diametrically opposed to the one encountered for the gluon case, i.e., it consists in a small increase of the saturation point. This result is also in harmony with what one would intuitively anticipate. In the SDE for the ghost, the quark propagator does not enter directly, but only through the gluon propagator or via higher loop corrections to the gluon-ghost vertex. Therefore, it is natural to expect the influence of dynamical quarks to be less pronounced for the ghosts.

(iii) When the gluon propagator obtained is used as an input in the ghost SDE, one finds that the requirement for the SDE solution to match the ghost propagator lattice data naturally provides a stringent check on the ghost-gluon vertex; specifically, this exercise will show that this vertex differs significantly from its tree-level value.

(iv) Finally, when all the results are used to form the RG invariant combination $\alpha\Delta F^2$ eventually leading to the QCD effective charge, we observe that, although obviously modifying the ultraviolet (UV) parameters controlling the running of the coupling and its magnitude, the number of fermions flavors does not affect the IR behavior of this quantity.

The paper is organized as follows: Sec. II provides the reader with some of the technical details of the lattice setup used for the computation of the relevant gluon and ghost Green functions. Next, in Sec. III, we present the results of the simulations, emphasizing the differences with respect to the quenched results; volume artifacts are also addressed in some detail. The ghost SDE is then solved in Sec. IV, and the effective coupling evaluated in Sec. V. Finally, we provide the conclusions in Sec. VI.

II. GENERALITIES

The following section is a reminder of how the ghost and gluon propagators are computed from the lattice simulations of gauge fields for light and heavy mass-twisted lattice flavors. It should be noticed that these propagators have been obtained (but not presented) earlier, as a by-product of the computation of the running coupling in the momentum (MOM) subtraction Taylor scheme [21]. These references, which the interested reader is referred to, also contain relevant details concerning lattice actions, setups and the treatment of artifacts.

In our simulations, the lattice fermion action for the doublet of light degenerate quarks is given by [22]

$$S_l = a^4 \sum_x \bar{\chi}_l(x)(D_W[U] + m_{0,l} + i\mu_l\gamma_5\tau_3)\chi_l(x), \qquad (2.1)$$

whereas, for the heavy doublet, we employ

$$S_h = a^4 \sum_x \bar{\chi}_h(x)(D_W[U] + m_{0,h} + i\mu_\sigma\gamma_5\tau_1 + \mu_\delta\tau_3)\chi_h(x), \qquad (2.2)$$

where $D_W[U]$ stands for the standard massless Wilson Dirac operator. In the gauge sector, the tree-level

[2]It should be also noticed that these $2 + 1 + 1$ configurations provide a realistic simulation of QCD below the bottom quark mass threshold, mainly at the momentum scales which we compute the Green functions for.

Symanzik improved gauge action [23] is applied for $N_f = 2$ and the Iwasaki improved action [24] for $N_f = 2 + 1 + 1$. In addition to the plaquette term $U^{1\times1}_{x,\mu,\nu}$, this formulation of the action also requires including rectangular (1×2) Wilson loops $U^{1\times2}_{x,\mu,\nu}$. For instance, in the tree-level Symanzik case, the action reads

$$S_g = \frac{\beta}{3}\sum_x \Bigg\{ b_0 \sum_{\substack{\mu,\nu=1\\ 1\le\mu<\nu}}^{4} [1 - \mathrm{Re}\,\mathrm{Tr}(U^{1\times1}_{x,\mu,\nu})] + b_1 \sum_{\substack{\mu,\nu=1\\ \mu\neq\nu}}^{4} [1 - \mathrm{Re}\,\mathrm{Tr}(U^{1\times2}_{x,\mu,\nu})] \Bigg\}, \tag{2.3}$$

where $\beta \equiv 6/g_0^2$, g_0 is the bare lattice coupling and one sets $b_1 = -1/12$ and $b_0 = 1 - 8b_1$ as dictated by the requirement of continuum limit normalization. Configurations of the gauge fields generated by the above actions are next gauge fixed to the (minimal) Landau gauge. This is done through the minimization of the following functional [of the $SU(3)$ matrices $U_\mu(x)$]

$$F_U[g] = \mathrm{Re}\Bigg\{ \sum_x \sum_\mu \mathrm{Tr}\Bigg[1 - \frac{1}{N} g(x) U_\mu(x) g^\dagger(x+\mu) \Bigg] \Bigg\}, \tag{2.4}$$

with respect to the gauge group element g.

To get as close as possible to the global minimum, we apply a combination of an over-relaxation algorithm and Fourier acceleration, considering the gauge to be fixed when the condition $|\partial_\mu A_\mu|^2 < 10^{-11}$ is fulfilled and the spatial integral of A_0 is constant in time to better than 10^{-6}. Evidently, this procedure cannot avoid the possibility that lattice Gribov copies are present in the ensemble of gauge fixed configurations. However, extensive literature in the quenched case (see for example Ref. [2]) shows that such copies do not seriously affect the qualitative and quantitative behavior of the Green functions in question. Given also the relative large physical volumes simulated, we will proceed under the working assumption that this feature survives unquenching, as was also verified in Ref. [13].

After the lattice configurations have been projected onto the Landau gauge, one can start calculating the Green functions of interest.

To begin with, we consider the gluon propagator. The gauge field is defined as

$$A_\mu(x + \hat{\mu}/2) = \frac{U_\mu(x) - U_\mu^\dagger(x)}{2iag_0} - \frac{1}{3}\,\mathrm{Tr}\frac{U_\mu(x) - U_\mu^\dagger(x)}{2iag_0}, \tag{2.5}$$

with $\hat{\mu}$ indicating the unit lattice vector in the μ direction. The two-point gluon Green function is then computed in momentum space through the following Monte Carlo average

$$\Delta^{ab}_{\mu\nu}(q) = \langle A^a_\mu(q) A^b_\nu(-q)\rangle = \delta^{ab}\Big(\delta_{\mu\nu} - \frac{q_\mu q_\nu}{q^2}\Big)\Delta(q^2), \tag{2.6}$$

with

$$A^a_\mu(q) = \frac{1}{2}\,\mathrm{Tr}\sum_x A_\mu(x + \hat{\mu}/2)\exp[iq\cdot(x+\hat{\mu}/2)]\lambda^a. \tag{2.7}$$

In the formula above λ^a are the Gell-Mann matrices and the trace is evaluated in color space.

The Landau gauge ghost propagator can also be computed in terms of Monte Carlo averages of the inverse of the Faddeev-Popov operator, i.e.,

$$F^{ab}(q^2) = \frac{1}{V}\Bigg\langle \sum_{x,y} \exp[iq\cdot(x-y)](M^{-1})^{ab}_{xy} \Bigg\rangle = \delta^{ab}\frac{F(q^2)}{q^2}, \tag{2.8}$$

with M written as a lattice divergence

$$M(U) = -\frac{1}{N}\nabla\cdot\tilde{D}(U), \tag{2.9}$$

and the operator $\tilde{D}$ acting on an arbitrary element of the Lie algebra η according to

$$\tilde{D}(U)\eta(x) = \frac{1}{2}[U_\mu(x)\eta(x+\mu) - \eta(x)U_\mu(x) + \eta(x+\mu)U_\mu^\dagger - U_\mu^\dagger(x)\eta(x)]. \tag{2.10}$$

More details on the lattice procedure for the inversion of the Faddeev-Popov operator can be found in Ref. [25].

Next, if we indicate with Λ the regularization cutoff (e.g., $\Lambda \equiv a^{-1}(\beta)$ if one specializes to lattice regularization), one can obtain the renormalized gluon propagator and ghost dressing function as

$$\begin{aligned} \Delta_{\mathrm{R}}(q^2,\mu^2) &= \lim_{\Lambda\to\infty} Z_3^{-1}(\mu^2,\Lambda^2)\Delta(q^2,\Lambda^2),\\ F_{\mathrm{R}}(q^2,\mu^2) &= \lim_{\Lambda\to\infty} \tilde{Z}_3^{-1}(\mu^2,\Lambda^2)F(q^2,\Lambda^2), \end{aligned} \tag{2.11}$$

where one imposes the standard MOM renormalization conditions

$$\Delta_{\mathrm{R}}(\mu^2,\mu^2) = 1/\mu^2, \qquad F_{\mathrm{R}}(\mu^2,\mu^2) = 1. \tag{2.12}$$

When unnecessary, we will refrain from explicitly indicating the renormalization point dependence of the various renormalized quantities.

We conclude this section by commenting briefly on the crucial role played by the so-called $H(4)$-extrapolation procedure [26], which have been used to correct the data for discretization artifacts (otherwise plaguing the reliable determination of Δ and F) due to the breaking of the $O(4)$ rotational invariance down to the $H(4)$ isometry group. Specifically, let us observe that the gluon and ghost

dressing functions ($q^2\Delta$ and F) are dimensionless correlation functions, and therefore general dimensional analysis shows that they must depend on the (dimensionless) lattice momentum aq_μ, where

$$q_\mu = \frac{2\pi n_\mu}{N_\mu a}, \qquad n_\mu = 0, 1, \ldots, N_\mu, \tag{2.13}$$

N_μ being the number of lattice sites in the μ direction (in our case, $N_x = N_y = N_z = N_t/2$). However, if one considers a dimensionless correlator Q evaluated on the lattice, since $O(4)$ is broken down to $H(4)$, one has

$$Q^{\text{latt}}\left(a^2q^2, a^2\frac{q^{[4]}}{q^2}, \cdots\right) = Q^{\text{latt}}(a^2q^2) + \left.\frac{\partial Q^{\text{latt}}}{\partial\left(a^2\frac{q^{[4]}}{q^2}\right)}\right|_{a^2\frac{q^{[4]}}{q^2}=0} a^2\frac{q^{[4]}}{q^2} + \cdots, \tag{2.14}$$

where $q^{[4]} = \sum_\mu q_\mu^4$ is the first $H(4)$ invariant (and the only one relevant in the ensuing analysis). The $H(4)$-extrapolation procedure is thought to account properly for the breaking of $O(4)$ down to $H(4)$ and thus recover the continuum limit $O(4)$ invariant result by means of the following prescription: one first averages over any combination of momenta being invariant under $H(4)$ (a so-called $H(4)$ orbit). Next, one extrapolates the results towards the continuum limit (where the effect of $a^2q^{[4]}$ must vanish) by applying Eq. (2.14) to all the orbits sharing the same value of q^2. The only assumption employed is that the slope coefficient in Eq. (2.14) depends smoothly on a^2q^2.

III. SIMULATION RESULTS

In this section we describe the outcome of our lattice simulations. The parameters used are reported in Table I. The physical scale, i.e., the lattice size at any bare coupling β, has been fixed by the ETM collaboration through chiral fits to lattice pseudoscalar masses and decay constants. At the physical point, these are required to take on the values of f_π and m_π provided by experiments. The bare untwisted mass is tuned to its critical value by setting the so-called untwisted partially conserved axial current mass to zero, so that the twisted-mass fermions are at *maximal twist*. The renormalized running masses for light and heavy quarks are obtained from the bare twisted mass as

$$\mu_{u,d}(q_0) = \frac{a\mu_l}{a(\beta)Z_P(q_0)}, \qquad \mu_{c/s}(q_0) = \frac{1}{a(\beta)Z_P(q_0)}\left(a\mu_\sigma \pm \frac{Z_S(q_0)}{Z_P(q_0)}a\mu_\delta\right), \tag{3.1}$$

where q_0 is the renormalization scale. The determination of the nonperturbative renormalization constants, in particular Z_P and Z_S, is the subject of an exhaustive computation program within the framework of the ETM collaboration (see for instance Ref. [27] for the $N_f = 2$ case and Refs. [28,29] which contain some preliminary results for the $N_f = 2 + 1 + 1$ case). The degenerate light quark masses we used for the simulations (Table I), range from 20 to 50 [MeV], while the strange quark is roughly set to 95 [MeV] and the heavy charm to 1.51 [GeV] (in $\overline{\text{MS}}$ at $q_0 = 2$ [GeV]). The lightest pseudoscalar masses for the simulations of Table I range approximately from 270 to 510 [MeV]. The biggest volume simulated corresponds to an asymmetrical box of roughly $3^3 \times 6$ [fm^4].

As previously mentioned, the MOM prescription (2.11) is to be applied if one wants to obtain the renormalized gluon and ghost propagators, which are the object of interest in the present work. Though they play a marginal role for our purposes, these constants have been computed at the subtraction point $\mu = 4.3$ GeV and, for the sake of completeness, collected in Table II.

TABLE I. Lattice setup parameters for the ensembles we used in this paper: κ_{crit} is the critical value for the standard hopping parameter for the bare untwisted mass; μ_l stands for the twisted mass for the two degenerated light quarks, while μ_σ and μ_δ define the heavy quarks twisted masses; and the last column indicates the number of gauge field configurations we used.

β	κ_{crit}	$a\mu_l$	$a\mu_\sigma$	$a\mu_\delta$	$(L/a)^3 \times T/a$	Configurations
3.90	0.161 856	0.004			$24^3 \times 64$	50
4.20	0.154 073	0.002			$48^3 \times 96$	50
1.95	0.161 240	0.0035	0.135	0.170	$48^3 \times 96$	40
1.90	0.163 270	0.0040	0.150	0.190	$32^3 \times 64$	50

TABLE II. MOM renormalization constants for ghost and gluon propagators computed at the subtraction point $\mu = 4.3$ GeV for the lattice parameters corresponding to the four ensembles described in Table I and used in this work.

β [N_f]	1.90 [2 + 1 + 1]	1.95 [2 + 1 + 1]	3.90 [2]	4.05 [2]
$Z_3(q_0 = 4.3\,\text{GeV})$	0.693(2)	0.709(2)	1.295(1)	1.341(3)
$\tilde{Z}_3(q_0 = 4.3\,\text{GeV})$	1.345(6)	1.38(2)	1.36(1)	1.37(1)

A. Gluon sector

The results obtained for the gluon propagator and dressing function for the cases of two light quarks and two light plus two heavy quarks are plotted[3] in Fig. 1. As far as the gluon propagator is concerned (top panel) one can clearly see the IR flattening typical of the massive solutions. However, when compared to the quenched case (shown for reference by the diamond-shaped gray data points), the propagator shows a less pronounced *swelling* at intermediate momenta and a lower freezing out value.

[3]If not stated otherwise we will be setting the renormalization point to be $\mu = 4.3$ GeV

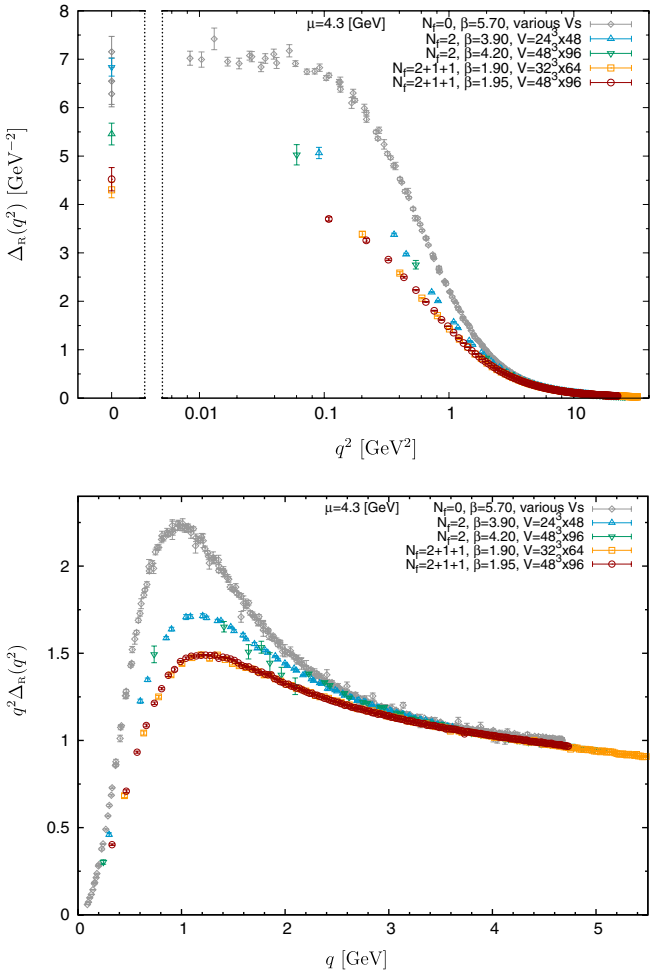

FIG. 1 (color online). The unquenched gluon propagator (top panel) and dressing function (bottom panel) for $N_f = 2$ (two light quarks) and $N_f = 2 + 1 + 1$ (two light and two heavy quarks). For the sake of comparison, in this and the following figures we plot the quenched data ($N_f = 0$) for various lattice volumes taken from Ref. [2]. The upper rhombus corresponds to $N_f = 0$, the intermediate up ($\beta = 3.90$) and down ($\beta = 4.20$) triangles to $N_f = 2$ and bottom circles ($\beta = 1.95$) and squares ($\beta = 1.90$) to $N_f = 2 + 1 + 1$.

To check the dependence of this latter effect on the lattice volume, we plot in Fig. 2 the value of $\Delta_R(0)$ as a function of the inverse of the volume. Though we do not have enough simulations on large volume lattices to attempt any continuum extrapolation, it is evident that residual volume effects are expected to be small when the appropriate simulations (i.e., $\beta = 4.20$ for $N_f = 2$ and both $\beta = 1.95$ and $\beta = 1.90$ for $N_f = 2 + 1 + 1$) are considered. Furthermore, apart from the zero-momentum gluon propagator, the results for our two simulations in both cases appear clearly superimposed in the plots of Fig. 1, indicating that volume effects are indeed under control.

In addition, the quenched simulation can be viewed as an unquenched counterpart in the limit of infinitely massive fermions, and the $N_f = 2$ results as the limit of the

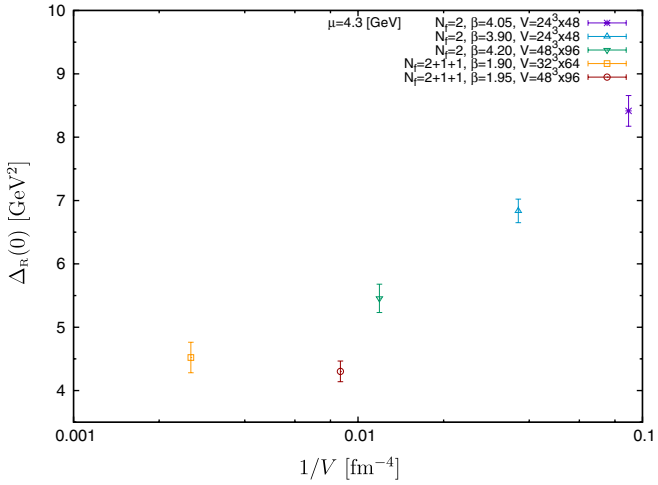

FIG. 2 (color online). The volume dependence of the IR saturation point of the gluon propagator $\Delta_R(0)$ in our simulations. For the $N_f = 2$ case, we include an extra point corresponding to a simulation on a $24^3 \times 48$ lattice, at $\beta = 4.05$ ($\kappa = 0.157010$ and $a\mu_l = 0.006$). Notice that this last point has not been exploited as it clearly corresponds to a very small physical volume. The upper rhombus corresponds to $N_f = 0$, the intermediate up ($\beta = 3.90$) and down ($\beta = 4.20$) triangles to $N_f = 2$ and bottom circles ($\beta = 1.95$) and squares ($\beta = 1.90$) to $N_f = 2 + 1 + 1$.

$N_f = 2 + 1 + 1$ case in the infinite mass limit of the heavy sector. Thus, one can unambiguously conclude that the presence of dynamical fermions suppresses the IR saturation point, and renders the gluon heavier. Also notice that the suppression tends to subside as the dynamical fermion mass increases. The decoupling of heavy fermions has been explicitly shown in the continuum through the SDE analysis of Ref. [8], where it was found that the gluon propagator results for $N_f = 2 + 1$ approach those for $N_f = 2$ as the mass of the heavy flavor is increased (see Fig. 17 of Ref. [8]).

Finally, the concave shape of the propagator ensures the violation of reflection positivity, thus implying that the unquenched gluon is also a confined excitation.

The behavior of the dressing function (bottom panel) is similar. In this case, the greater the number of dynamical quarks, the less pronounced the peak at the intermediate momenta. Analogously, the heavier the quark, the less the effect it entails on the overall shape of the dressing function. These results are in agreement with the SDE study of Ref. [8], as well as with the lattice findings of Refs. [11–13].

B. Ghost sector

The results for the ghost dressing function are plotted in the top panel of Fig. 3. In analogy with the quenched case, the data do not support a powerlike singular behavior in the (deep) IR region, rather one finds the characteristic freezing out feature of the massive solutions [4,30]. As one

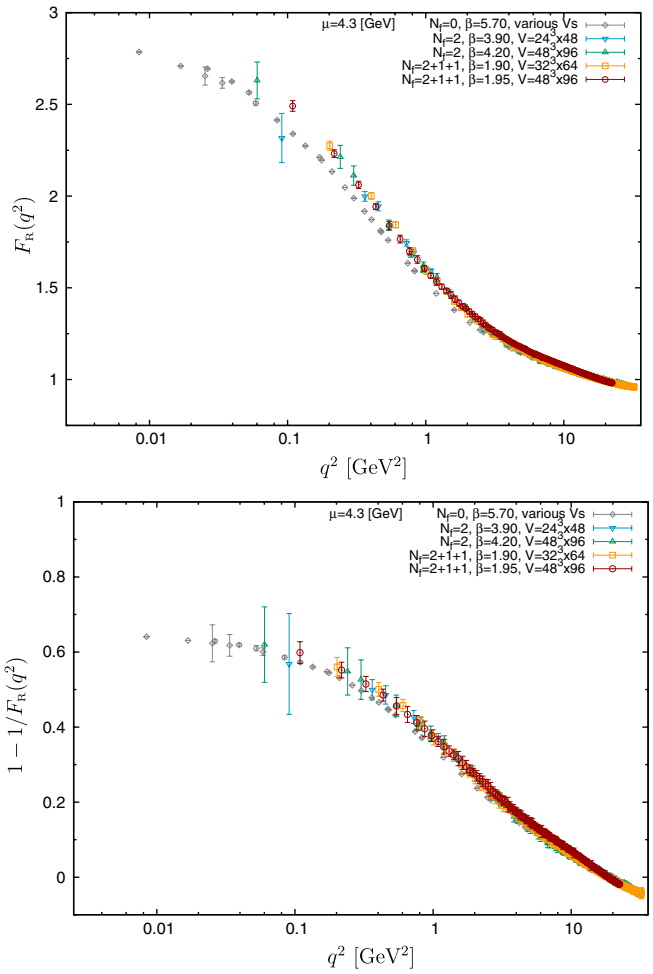

FIG. 3 (color online). The unquenched ghost dressing function (top panel) and the (approximate) Kugo-Ojima function (bottom panel) for $N_f = 2$ (two light quarks) and $N_f = 2 + 1 + 1$ (two light and two heavy quarks). The quenched ($N_f = 0$) data shown in this and the following figures are again taken from Ref. [2]. The upper rhombus corresponds to $N_f = 0$, the intermediate up ($\beta = 3.90$) and down ($\beta = 4.20$) triangles to $N_f = 2$ and bottom circles ($\beta = 1.95$) and squares ($\beta = 1.90$) to $N_f = 2 + 1 + 1$.

would expect on the basis of a naive perturbative analysis (there is no tree-level coupling between ghosts and fermions) the effect of dynamical quarks on the ghost sector is much milder as compared to the gluon sector.

The ghost dressing function F can provide valuable information with respect to the so-called Kugo-Ojima function [18]. This is due to a powerful identity dictated by the underlying Becchi-Rouet-Stora-Tyutin symmetry present in the continuum formulation of the theory, which leads to the relation [31,32]

$$F^{-1}(q^2) = 1 + G(q^2) + L(q^2), \tag{3.2}$$

where $G(q^2)$ and $L(q^2)$ are the form factors of a particular Green function $\Lambda_{\mu\nu}(q)$ that plays a special role in the aforementioned PT-BFM truncation scheme [33], with

$$\Lambda_{\mu\nu}(q) = \delta_{\mu\nu} G(q^2) + \frac{q_\mu q_\nu}{q^2} L(q^2). \tag{3.3}$$

The important point here is that $G(q^2)$ coincides (in the Landau gauge) with the Kugo-Ojima function [31,32]. In addition, a detailed analysis of the $L(q^2)$ form factor in the quenched approximation reveals that it is numerically subdominant in the whole range of momenta when compared to $G(q^2)$ [32], and, furthermore, $L(0) = 0$. Since quark effects on $\Lambda_{\mu\nu}(q)$ are suppressed, either due to their indirect presence in the full gluon and ghost propagators, or in higher order corrections to the ghost-gluon kernel (the first one happening at the three-loop level in the kernel skeleton expansion, and therefore at four loops in $\Lambda_{\mu\nu}$), one naturally expects the same results to survive in the unquenched case, thus leaving us with the approximate relation

$$G(q^2) \approx F^{-1}(q^2) - 1. \tag{3.4}$$

In the bottom panel of Fig. 3 we plot the function $-G(q^2)$ and observe that its value at origin is practically unchanged when varying the number of flavors. Clearly the behavior is not dissimilar from the one revealed in quenched simulation, and the (extrapolated) IR saturation value looks once again far from the critical value 1 predicted by the scaling type solutions of the SDE and the related Kugo-Ojima confinement criterion. We will return to this issue in the next section.

IV. GHOST SDE ANALYSIS

In this section we carry out a hybrid analysis combining our lattice simulation results with SDE techniques, in a spirit analogous to what has been reported in Ref. [30]. The aim is to study the ghost sector in greater detail and, in particular, gain access to the ghost-gluon vertex form factor(s). As a welcome byproduct, we will obtain a reliable extrapolation of the ghost lattice data to the deep IR.

Specifically, let us start by considering the ghost SDE, which can be recast in the following bare form

$$\frac{1}{F(q^2)} = 1 + g_0^2 N_c \int \frac{d^4k}{(2\pi)^4} \frac{F(k^2)\Delta((k-q)^2)}{k^2(k-q)^2} \times \left[\frac{(q\cdot k)^2}{q^2} - k^2\right] H_1(k,q), \tag{4.1}$$

where $H_1(k, q)$ is nonlongitudinal form factor of the ghost-gluon vertex, parameterized as

$$\begin{aligned}\tilde{\Gamma}^{abc}_{\nu}(-k, q; k-q) &= i g_0 f^{abc} k_{\nu'} \tilde{\Gamma}_{\nu'\nu}(-k, q; k-q) \\ &= i g_0 f^{abc} [k_\nu H_1(k,q) \\ &\quad + (k-q)_\nu H_2(k,q)],\end{aligned} \tag{4.2}$$

with k and q being the outgoing and incoming ghost momenta, respectively, and g_0 the bare coupling constant. As explained in depth in Refs. [30,34,35], one can first renormalize the ghost and gluon propagators in Eq. (4.1),

by using Eq. (2.12), and then apply a subtraction procedure to deal with the UV singularity of the ghost self-energy integral to obtain

$$\frac{1}{F_{\mathrm{R}}(q^2)} = 1 + \tilde{Z}_3^2 Z_3 \frac{g_0^2}{4\pi} \int k^3 \mathrm{d}k K(k,q) H_1^{\mathrm{bare}}(k,q) F_R(k^2), \tag{4.3}$$

where

$$K(k,q) = -\frac{1}{\pi^2} \int_0^\pi \sin^4\theta \mathrm{d}\theta \left[\frac{\Delta_R((k-q)^2)}{(k-q)^2} - \frac{\Delta_R((k-p)^2)}{(k-p)^2} \right]. \tag{4.4}$$

The renormalization point, μ^2, is implicitly present as an argument for all the renormalized quantities. In obtaining Eq. (4.3), the subtraction procedure is applied for Eq. (4.1) evaluated at the two momenta k and p, both being parallel and such that $p^2 = \mu^2$. H_1 in Eq. (4.3) is a bare but finite [36] quantity which needs no renormalization while, in front of the integral, the renormalization constants and the bare coupling especially appear in the right combination to cancel the cutoff dependence and give the MOM Taylor scheme coupling (see, e.g., Ref. [20]),

$$\alpha_{\mathrm{T}}(\mu^2) = \frac{g_0^2}{4\pi} \tilde{Z}_3^2(\mu^2) Z_3(\mu^2). \tag{4.5}$$

This coupling $\alpha_{\mathrm{T}}(\mu^2)$ for $N_f = 0$, 2 and $2+1+1$ can be determined from lattice data (see, e.g., Refs. [20,21]). In order to solve the ghost SDE in isolation (i.e., without coupling it to the much more complicated gluon SDE), one can use the just determined lattice gluon propagator Δ_{R} as an input for the equation, thus fully determining the kernel (4.4). Now the only unknown term present in the equation is the ghost form factor H_1; clearly the solutions to the ghost SDE will describe the lattice data with a better or worse agreement depending on our ability to model this form factor [17,37].

Through the analysis of the quenched lattice data, it was shown in Ref. [30] that the solutions of Eq. (4.3) grossly underestimate (by a factor of at least 2) the lattice data if one uses the tree-level value $H_1 = 1$ for the ghost-gluon form factor. A constant does indeed do a better job [30] but does not allow for a precise description of the deep IR behavior of the function [17]. This implies that a good description of the (quenched) ghost dressing lattice data calls for a ghost-gluon form factor with a nontrivial kinematical structure. Using the knowledge derived from the operator product expansion (OPE) analysis of Ref. [17], coupled with the current lattice data on the (Landau gauge) ghost-gluon vertex [38], one can parameterize this form factor as[4]

$$H_1(k,0) = H_1^0 \left[1 + \frac{N_C g^2 \langle A^2 \rangle}{4(N_C^2-1)} \frac{k^2}{k^4 + m_{\mathrm{IR}}^4} \right] + (1 - H_1^0) \left[\frac{w^4}{w^4 + k^4} \right]. \tag{4.6}$$

Estimates for the gluon condensate[5] $g^2\langle A^2\rangle$, and the IR mass scale m_{IR}, can be obtained from lattice data and OPE analysis [37]; the constants H_1^0 and w (introduced in order to guarantee that $H_1(0,0) = 1$, as suggested by current lattice data [38]) can be adjusted so that the solutions Eq. (4.3) match the corresponding lattice data as closely as possible.

The solutions of the ghost SDE (4.3) following the procedure just illustrated are presented in Fig. 4. In the top panel of the figure one can clearly see that, similarly to the quenched case, a tree-level value for H_1 does not give solutions which can describe the lattice data. However, once the kinematically nontrivial expression, Eq. (4.6) (bottom panel of the same figure), is included in the equation, one obtains an excellent agreement with the data. Therefore, effectively, the curves for $H_1(q,0)$ represent a genuine prediction of our analysis; it would therefore be extremely interesting to confirm or refute this prediction through direct lattice calculations of the ghost-gluon three-point function. It should be noticed that, when obtaining the dressing function from the ghost SDE, the subtraction point has been fixed at $\mu = 3.61$ GeV (the same happens in Fig. 4). This is merely aimed to allow for a direct comparison with the quenched analysis of Refs. [30,39]. Of course, once the dressing function renormalized at a given μ is obtained, it can be renormalized at any other point μ' through the simple rescaling

$$F_{\mathrm{R}}(q^2, \mu'^2) = \frac{F_{\mathrm{R}}(q^2,\mu^2)}{F_{\mathrm{R}}(\mu'^2,\mu^2)}, \tag{4.7}$$

where the second argument of F specifies the renormalization point. Equation (4.7) is applied to obtain the SDE ghost dressing prediction for $\mu' = 4.3$ GeV in Fig. 5 and in the following section. To be sure, it can be straightforwardly proven that $F_R(q^2,\mu'^2)$, given by Eq. (4.7), is a solution of the ghost SDE in Eq. (4.3) when $g_0^2(\mu^2)$ is replaced by[6]

$$g_0^2(\mu'^2) = g_0^2(\mu^2) F_{\mathrm{R}}^2(\mu'^2,\mu^2) \mu'^2 \Delta(\mu'^2,\mu^2), \tag{4.8}$$

which gives the perturbative renormalization flow of the Taylor coupling, as can be inferred from Eq. (4.5).

[4]Equation (4.3) requires to be solved with the full vertex $H_1(k,q)$, which is modeled in Ref. [17]; however, it can be shown that $H_1(k,q) \simeq H_1(k,0)$ is a good approximation to obtain the ghost dressing in the IR momentum region [39].

[5]The very notion of condensate have been recently questioned in Refs. [40,41]. In particular, according to the new perspective suggested there, our gluon condensate $g^2\langle A^2\rangle$ should be understood as a mass-scale parameter related to the local operator A^2 in the OPE expansion of the gluon Green functions.

[6]Observe that the unity appearing on the rhs of Eq. (4.3) has also to be replaced by $1/F_{\mathrm{R}}(\mu^2,\mu'^2)$.

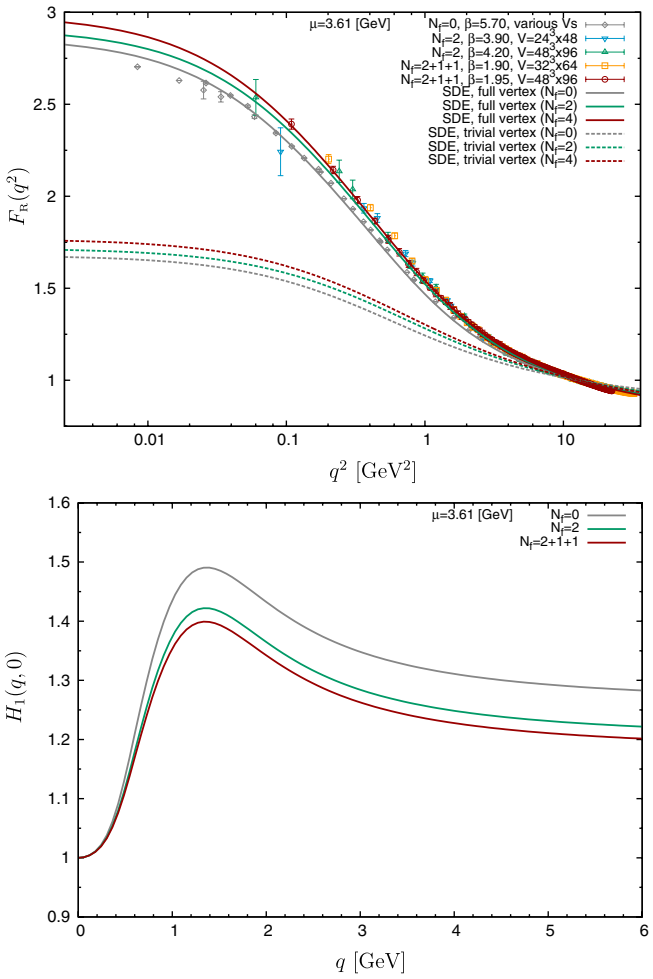

FIG. 4 (color online). Top panel: The ghost dressing function obtained from the solution of the ghost SDE (4.3) with the lattice gluon propagator as an input and $\alpha_T = 0.25, 0.32, 0.37$, respectively, for $N_f = 0$, 2, and $2 + 1 + 1$ at $\mu = 3.61$ [GeV]. Dashed lines correspond to solutions for the tree-level $H_1(q, 0) = 1$, while continuous lines to the inclusion of the full form factor (4.6). The latter is also shown in the bottom panel. The values of the parameters used to integrate the ghost SDE are: $g^2\langle A^2\rangle = 7$ GeV^2, $m_{IR} = 1.3$ GeV and $w = 0.65$ GeV (the same IR ones for the three cases). Moreover, $H_1^0 = 1.26$, 1.20, 1.18 for $N_f = 0$, 2 and $2 + 1 + 1$, respectively upper curve correspond to $N_f = 0$, intermediate to $N_f = 2$ and bottom one to $N_f = 2 + 1 + 1$.

The good agreement between the SDE solutions and the lattice data allows for an extrapolation of the latter towards the deep IR region, where one observes a very small increment of the saturation point (monotonic with N_f). In particular, the extrapolated zero-momentum values for the ghost dressing function, renormalized at $\mu = 4.3$ GeV, are given by 2.86, 2.91, and 2.98 for $N_f = 0$, 2 and $2 + 1 + 1$, respectively. This SDE-driven extrapolation is particularly useful when scrutinizing the Kugo-Ojima function of Fig. 5, which clearly shows that the saturation point of this function is practically insensitive to the inclusion of dynamical fermions.

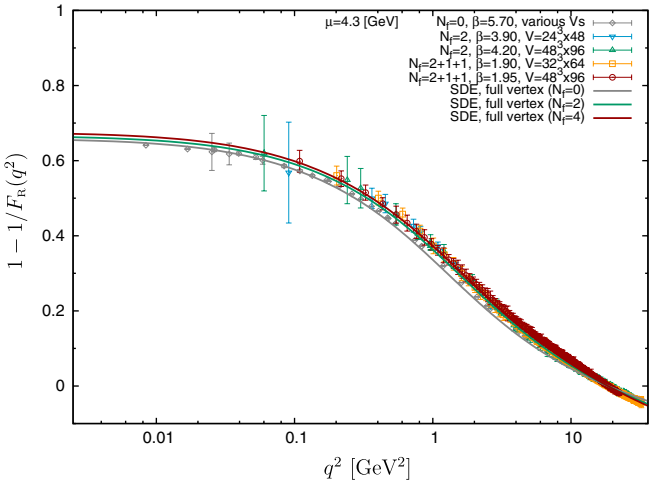

FIG. 5 (color online). Extrapolation of the (approximate) Kugo-Ojima function in the deep IR. The ghost dressing function F employed in this plot is generated by solving the ghost SDE. The upper rhombus corresponds to $N_f = 0$, the intermediate up ($\beta = 3.90$) and down ($\beta = 4.20$) triangles to $N_f = 2$ and bottom circles ($\beta = 1.95$) and squares ($\beta = 1.90$) to $N_f = 2 + 1 + 1$.

V. EFFECTIVE COUPLING

The results obtained for the gluon and ghost two-point functions allow us to extract the running of the full QCD effective charge for a wide range of physical momenta, and in particular in the deep IR region which is evidently inaccessible to perturbation theory.

To begin with, let us recall that the QCD effective charge is defined, among practitioners, in primarily two different ways: the first one (to be denoted by α_{PT}) is obtained within the framework of the pinch technique [9,42] and represents the most direct generalization of the familiar QED effective charge concept to a non-Abelian setting; the second one (to be denoted by α_{gh}) corresponds to the nonperturbative generalization of the strong coupling in the Taylor scheme mentioned before [21].

The construction of either effective charges proceeds through the identification of a suitable RG invariant combination. Before identifying this quantity, however, let us observe that though the effective couplings α_{PT} and α_{gh} have a rather distinct theoretical origin and status, it turns out that in the Landau gauge, they are related through the equation [19]

$$\alpha_{gh}(q^2) = \left[1 + \frac{L(q^2)}{1 + G(q^2)}\right]^{-2} \alpha_{PT}(q^2). \tag{5.1}$$

Evidently, in the approximation $L(q^2) \approx 0$, used throughout this paper, the two definitions coincide, and one has $\alpha_{PT}(q^2) \equiv \alpha_{gh}(q^2) \equiv \bar{\alpha}(q^2)$. This implies also that one can choose as the RG invariant combination

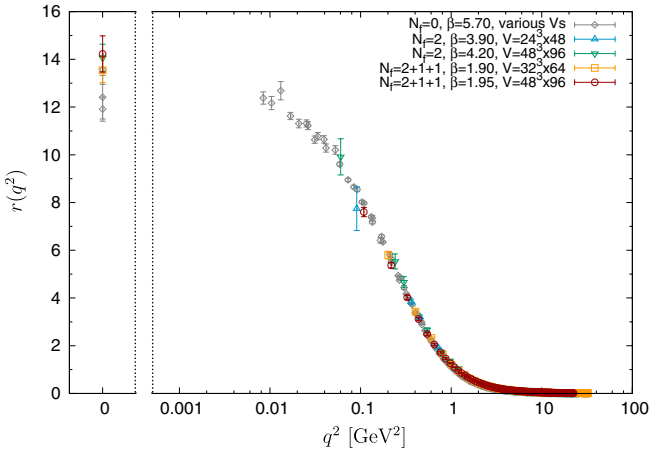

FIG. 6 (color online). The RG invariant quantity $r(q^2)$ defined in Eq. (5.2) for the different values of flavors N_f. Errors for the $N_f = 0$ case are underestimated, since we have used the ghost dressing function obtained from the SDE for constructing the effective charge. Notice the absence of any flavor dependence below the 1 GeV region. The upper rhombus corresponds to $N_f = 0$, the intermediate up ($\beta = 3.90$) and down ($\beta = 4.20$) triangles to $N_f = 2$ and bottom circles ($\beta = 1.95$) and squares ($\beta = 1.90$) to $N_f = 2 + 1 + 1$.

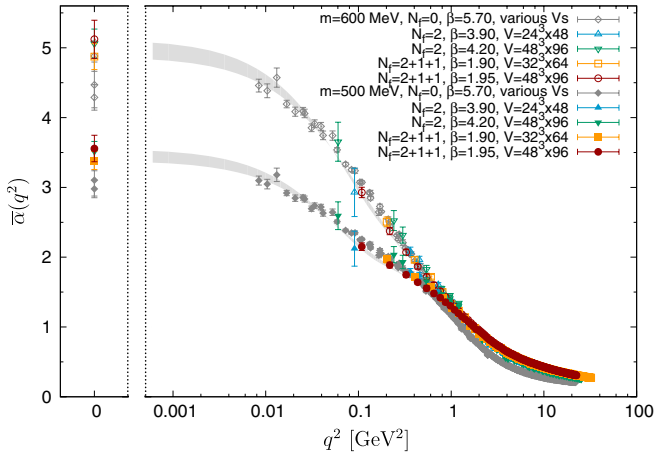

FIG. 7 (color online). The effective charge $\bar{\alpha}(q^2)$ defined in Eq. (5.3) for two different values of the IR gluon mass: $m_0 = 500$ MeV (solid symbols) and $m_0 = 600$ MeV (open symbols). The gray band in the background (meant to guide the eye) has been obtained from a continuum extrapolation of the $N_f = 2 + 1 + 1$ data. The upper rhombus corresponds to $N_f = 0$, the intermediate up ($\beta = 3.90$) and down ($\beta = 4.20$) triangles to $N_f = 2$ and bottom circles ($\beta = 1.95$) and squares ($\beta = 1.90$) to $N_f = 2 + 1 + 1$.

$$r(q^2) = \alpha_{\mathrm{T}}(\mu^2)\Delta_{\mathrm{R}}(q^2, \mu^2)F_{\mathrm{R}}^2(q^2, \mu^2), \qquad (5.2)$$

which can be readily obtained from the data presented so far [α_{T} is given in Eq. (4.5)]. The quantity $r(q^2)$ defined above is constructed in Fig. 6 for different number of flavors N_f; notice that for calculating the freezing out point $r(0)$ the value of $F_{\mathrm{R}}(0)$ has been extrapolated from the SDE results for the ghost dressing obtained in the previous section.

A most salient feature of this plot is the absence (within the errors) of any flavor dependence in the IR region, more precisely starting from $q^2 \lesssim 1$ GeV^2. Indeed, one observes that the flavor effects which control the behavior of the UV parameters of the theory (e.g., the β-function coefficients, Λ_{QCD} and $\langle A^2 \rangle$), combine in such a way that, when the RG invariant combination $r(q^2)$ is formed, no net flavor dependence survives in the IR.

Since, modulo an overall dimensionful factor to render it dimensionless, $r(q^2)$ coincides with the effective coupling, the origin of this independence can be understood by recalling the reason for the N_f dependence of the running coupling in the UV (it should also be noticed that the invariant combination $r(q^2)$ is related with the UV coupling defined through the ghost-gluon vertex in Taylor scheme by nothing but a factor q^2). In this case the bigger the physical momenta q^2, the more channels open up for the production of quark-antiquark virtual pairs (so that every time a channels opens, the coupling receives a *kick* and goes up). However, as soon as q^2 drops below a certain threshold, no energy will be available to produce any virtual pairs (not even gluons when $q_0^2 < 4m_0^2$) so that the residual running of the coupling below this value is completely dominated by the IR mass scale introduced when defining the effective charge.

Coming to this specific point, it turns out that [19] one can construct from $r(q^2)$ the dimensionless effective coupling $\bar{\alpha}(q^2)$ by pulling out the inverse propagator factor $q^2 + m^2(q^2)$, i.e.,

$$\bar{\alpha}(q^2) = [q^2 + m^2(q^2)]r(q^2), \qquad (5.3)$$

which leads to an IR saturating coupling. Notice that this definition is valid for both massive and the (already ruled out) scaling solutions (in which case one would have to set $m^2(q^2) = 0$); since in the latter case $\Delta(0) \to 0$ and $F(0) \to \infty$, the effective coupling does not distinguish between the two solutions.[7]

As a last step, we need to specify the q^2 running of the dynamical mass $m^2(q^2)$. We will consider here the simplified setting of Refs. [19,43] under which the mass obeys a power law running

$$m^2(q^2) = \frac{m_0^4}{q^2 + m_0^2}, \qquad m_0 \equiv m(0), \qquad (5.4)$$

and for m_0 one considers the representative values $m_0 = 500$–600 MeV, consistent with a variety of

[7]As explained in detail in Ref. [19], in the presence of an IR saturating propagator, one should not insist in pulling out in front of the effective coupling a simple q^2 factor. Otherwise, one would end up with a completely unphysical coupling, namely the one that vanishes in the IR, where QCD is supposed to be a strongly coupled theory.

phenomenological studies. The resulting effective charge is plotted in Fig. 7.

We hasten to emphasize that this is only a toy model, and one should take into account that in reality m_0 differs for different N_f, as clearly seen in the top panel of Fig. 1. However, inserting directly in Eq. (5.4) the saturation value $m_0 = \Delta_R^{-1}(0, \mu^2)$ obtained from our simulations for different number of flavors N_f, breaks the RG invariance in zero of Eq. (5.3).[8] We are evidently in need of better tools for extracting reliable (RG invariant) information about the saturation point of the coupling (and probably more data as well in the low momentum region); this issue clearly deserves a separate study.

VI. CONCLUSIONS

In this paper, we have carried out a systematic and comprehensive analysis of the gluon and ghost two-point functions in (Landau gauge) full lattice QCD.

The configurations used include two light and two light plus two heavy twisted mass fermions with masses between 20–50 [MeV] for the light quarks, 95 [MeV] for the strange quark and 1.51 [GeV] for the charm quark (in $\overline{\text{MS}}$ scheme at a renormalization scale of 2 [GeV]). The mass of the lightest pseudoscalar turns out to be between the range of 270 and 510 [MeV]. As this value does not lie too far from the physical pion mass, it increases our confidence in the flavor physics effects reported in this article. Moreover, simulations on lattices with up to $48^3 \times 96$ points, with $\beta = 3.90$ and 4.20 for $N_f = 2$ and $\beta = 1.90$ and 1.95 for $N_f = 2 + 1 + 1$, allow us to reach momenta down to $q \simeq 300$ [MeV], keeping the volume effects under control.

Our analysis demonstrates that in the intermediate and low momentum region, the gluon propagator lessens with the increase in the number of dynamical quarks, whereas, the ghost dressing function is enhanced, albeit only slightly. In addition, the heavier a species of fermions, the smaller in extent is its effect on the suppression of the gluon propagator. With a heavier enough mass, which prevents its virtual pair production, the fermion fails to screen the interaction and gets decoupled from the gluon dynamics altogether.

When all the pieces of data are put together to construct the effective QCD running coupling, $\bar{\alpha}(q^2)$, we observe the behavior anticipated from the massive decoupling solutions, namely, a monotonic approach to an IR fixed point. Furthermore, we find that below $q \simeq 1$ [GeV], this quantity is not directly affected by the variation in the number of dynamical fermion flavors. However, considering that an IR gluon mass is introduced while defining the effective running coupling, there is indirect dependence on N_f via this mass scale.

Making the most of the lattice results for the gluon and ghost propagators, we present a self-consistent analysis of the ghost 2-point function and extract the unquenched ghost-gluon form factor H_1. This is a genuine prediction of the SDE study presented in Sec. IV, which should be confirmed (or refuted) through direct lattice studies of the ghost-gluon vertex.

Evidently, while the whole analysis in the present paper has been performed in the Landau gauge, the gluon and ghost propagators are gauge dependent quantities and one might wonder how the results reported will change when considering other gauges.[9] To begin with, the IR saturation point of the gluon propagator and the ghost dressing function obtained for the different number of flavors N_f are particular to the Landau gauge, and one should not expect that the *same* points would emerge had one carried out the simulation in a different gauge (e.g., the Feynman gauge). However, the fact that the PT-BFM framework carries over practically unmodified to both R_ξ and background field covariant gauges, gives good reasons to expect that the IR finiteness found in the quenched as well as in the unquenched (Landau gauge) cases, will persist in this class of gauges.[10] In this respect, very preliminary results on lattice calculations performed within an R_ξ gauge with $\xi \neq 0$ have appeared in the literature [45], while recently, a gauge fixing functional has been derived in Refs. [46,47], which, upon a suitable minimization procedure, gives the background Landau gauge condition; it will be therefore extremely interesting to compare the Landau gauge results, with Green's functions obtained from (large volume) lattice configurations gauge fixed using these new implementations.[11] A qualitatively different picture may finally appear in the context of noncovariant gauge fixing schemes, such as the Coulomb gauge or the maximal Abelian gauge [48]; for instance, in the former gauge, only *scaling* solutions (for which $\Delta(0) = 0$) have been reported from both SDE and lattice analysis [49].

[8]One could in principle choose different phenomenological values of m_0 for different values of N_f but the result would not be that different from what is seen in Fig. 7.

[9]Notice that, away from the Landau gauge, the whole notion of a Kugo-Ojima function and the corresponding confinement criterion becomes meaningless.

[10]In particular, the PT-BFM analysis of Ref. [44] predicts a finite ghost *propagator* in the Feynman gauge, while a prediction for the gluon propagator in the *background* Landau gauge can be found in Ref. [32]. From a lattice perspective, in both cases the concave gluon propagator shape points towards a violation of the reflection positivity thus preventing the gluon from being considered a free state.

[11]In the BFM case, one obstacle that need to be overcome before full lattice simulations can be realized is to devise a lattice algorithm which would allow to treat the background field as an external yet unspecified source, so that it could be set to zero at the end of the calculation.

We conclude by observing that, though the data presented have been obtained for an arbitrary gauge copy selected through a gauge fixing algorithm using a combination of over-relaxation and Fourier acceleration, we do not expect that the presence of Gribov copies to alter the conclusions in any significant way, given also that their effect is expected to weaken significantly for physical volumes as large as the ones considered here.

ACKNOWLEDGMENTS

A. B. wishes to acknowledge the financial grants CONACyT Project No. 46614-F and Coordinación de la Investigación Científica (CIC) Project No. 4.10 and U.S. Department of Energy, Office of Nuclear Physics, Contract No. DE-AC02-06CH11357. The work of M. C. is supported by the AuroraScience project, which is funded jointly by the Provincia Autonoma di Trento (PAT) and the Istituto Nazionale di Fisica Nucleare (INFN). Part of the calculations were performed using the Aurora Supercomputer at the Fondazione Bruno Kessler (Trento). J. R.-Q. is indebted to O. Pène, Ph. Boucaud, B. Blossier, K. Petrov and C. D. Roberts for fruitful discussions and very helpful comments, and also acknowledges the Spanish MICINN for the support by the Research Project No. FPA2011-23781 and ''Junta de Andalucia'' by Project No. P07FQM02962.

[1] A. Cucchieri and T. Mendes, Proc. Sci., LAT2007 (2007) 297; QCD-TNT09 (2009) 026; O. Oliveira and P. Silva, Proc. Sci., LAT2009 (2009) 226; I. Bogolubsky, E.-M. Ilgenfritz, M. Muller-Preussker, and A. Sternbeck, Proc. Sci., LAT2007 (2007) 290.

[2] I. Bogolubsky, E.-M. Ilgenfritz, M. Muller-Preussker, and A. Sternbeck, Phys. Lett. B **676**, 69 (2009).

[3] A. C. Aguilar, D. Binosi, and J. Papavassiliou, Phys. Rev. D **78**, 025010 (2008).

[4] P. Boucaud, J. Leroy, A. L. Yaouanc, J. Micheli, O. Pène, and J. Rodríguez-Quintero, J. High Energy Phys. 06 (2008) 099.

[5] C. S. Fischer, A. Maas, and J. M. Pawlowski, Ann. Phys. (Berlin) **324**, 2408 (2009).

[6] D. Dudal, J. A. Gracey, S. P. Sorella, N. Vandersickel, and H. Verschelde, Phys. Rev. D **78**, 065047 (2008).

[7] A. Bashir, L. Chang, I. Cloet, B. El-Bennich, Y.-X. Liu, C. D. Roberts, and P. C. Tandy, Commun. Theor. Phys. **58**, 79 (2012).

[8] A. Aguilar, D. Binosi, and J. Papavassiliou, Phys. Rev. D **86**, 014032 (2012).

[9] A. C. Aguilar and J. Papavassiliou, J. High Energy Phys. 12 (2006) 012; D. Binosi and J. Papavassiliou, Phys. Rev. D **77**, 061702 (2008); J. High Energy Phys. 11 (2008) 063; Phys. Rep. **479**, 1 (2009).

[10] C. S. Fischer and R. Alkofer, Phys. Rev. D **67**, 094020 (2003).

[11] P. O. Bowman U. Heller, D. Leinweber, M. Parappilly, A. Sternbeck, L. von. Smekal, A. Williams, and J. Zhang, Phys. Rev. D **76**, 094505 (2007).

[12] W. Kamleh, P. O. Bowman, D. B. Leinweber, A. G. Williams, and J. Zhang, Phys. Rev. D **76**, 094501 (2007).

[13] E.-M. Ilgenfritz, M. Muller-Preussker, A. Sternbeck, A. Schiller, and I. Bogolubsky, Braz. J. Phys. **37**, 193 (2007).

[14] R. Baron, P. Boucaud, J. Carbonell, A. Deuzeman, V. Drach *et al.* (ETM Collaboration), J. High Energy Phys. 06 (2010) 111.

[15] R. Baron, B. Blossier, P. Boucaud, J. Carbonell, A. Deuzeman *et al.* (ETM Collaboration), Proc. Sci., LATTICE2010 (2010) 123.

[16] R. Frezzotti, P. A. Grassi, S. Sint, and P. Weisz (ALPHA Collaboration), J. High Energy Phys. 08 (2001) 058.

[17] P. Boucaud, J. Leroy, A. L. Yaouanc, J. Micheli, O. Pene, and J. Rodríguez-Quintero, Few-Body Syst. **53**, 387 (2012).

[18] T. Kugo and I. Ojima, Prog. Theor. Phys. Suppl. **66**, 1 (1979).

[19] A. C. Aguilar, D. Binosi, J. Papavassiliou, and J. Rodriguez-Quintero, Phys. Rev. D **80**, 085018 (2009).

[20] P. Boucaud, F. De Soto, J. Leroy, A. L. Yaouanc, J. Micheli, O. Pène, and J. Rodríguez-Quintero, Phys. Rev. D **79**, 014508 (2009).

[21] B. Blossier, P. Boucaud, F. De soto, V. Morenas, M. Gravina, O. Pène, and J. Rodríguez-Quintero (ETM Collaboration), Phys. Rev. D **82**, 034510 (2010); B. Blossier, P. Boucaud, M. Brinet, F. De Soto, X. Du, M. Gravina, V. Morenas, O. Pène, K. Petrov, and J. Rodríguez-Quintero, Phys. Rev. D **85**, 034503 (2012); Phys. Rev. Lett. **108**, 262002 (2012).

[22] R. Frezzotti and G. C. Rossi, Nucl. Phys. B, Proc. Suppl. **128**, 193 (2004).

[23] P. Weisz, Nucl. Phys. **B212**, 1 (1983).

[24] Y. Iwasaki, Nucl. Phys. **B258**, 141 (1985); Y. Iwasaki, K. Kanaya, T. Kaneko, and T. Yoshie, Phys. Rev. D **56**, 151 (1997).

[25] P. Boucaud, J. Leroy, A. L. Yaouanc, A. Lokhov, J. Micheli, O. Pène, J. Rodríguez-Quintero, and C. Roiesnel, Phys. Rev. D **72**, 114503 (2005).

[26] D. Becirevic, P. Boucaud, J. Leroy, J. Micheli, O. Pene, J. Rodriguez-Quintero, and C. Roiesnel, Phys. Rev. D **60**, 094509 (1999); **61**, 114508 (2000); F. de Soto and C. Roiesnel, J. High Energy Phys. 09 (2007) 007.

[27] R. Baron *et al.* (ETM Collaboration), J. High Energy Phys. 08 (2010) 097.

[28] B. Blossier, P. Boucaud, M. Brinet, F. De Soto, X. Du *et al.*, Proc. Sci., LAT2011 (2011) 223.

[29] B. Blossier *et al.* (ETM Collaboration), Proc. Sci., LAT2011 (2011) 233.

[30] P. Boucaud, J.-P. Leroy, A. Yaouanc, J. Micheli, O. Pène, and J. Rodríguez-Quintero, J. High Energy Phys. 06 (2008) 012.
[31] P. A. Grassi, T. Hurth, and A. Quadri, Phys. Rev. D **70**, 105014 (2004).
[32] A. C. Aguilar, D. Binosi, and J. Papavassiliou, J. High Energy Phys. 11 (2009) 066.
[33] D. Binosi and J. Papavassiliou, Phys. Rev. D **66**, 025024 (2002).
[34] P. Boucaud, M. Gomez, J. Leroy, A. L. Yaouanc, J. Micheli, O. Pène, and J. Rodríguez-Quintero, Phys. Rev. D **82**, 054007 (2010).
[35] J. Rodriguez-Quintero, J. High Energy Phys. 01 (2011) 105.
[36] J. Taylor, Nucl. Phys. **B33**, 436 (1971).
[37] P. Boucaud, D. Dudal, J. Leroy, O. Pene, and J. Rodriguez-Quintero, J. High Energy Phys. 12 (2011) 018.
[38] A. Maas, A. Cucchieri, and T. Mendes, Braz. J. Phys. **37**, 219 (2007).
[39] D. Dudal, O. Oliveira, and J. Rodriguez-Quintero, arXiv:1207.5118.
[40] S. J. Brodsky, C. D. Roberts, R. Shrock, and P. C. Tandy, Phys. Rev. C **82**, 022201 (2010).
[41] L. Chang, C. D. Roberts, and P. C. Tandy, Phys. Rev. C **85**, 012201 (2012).
[42] J. M. Cornwall, Phys. Rev. D **26**, 1453 (1982).
[43] A. Aguilar, D. Binosi, and J. Papavassiliou, J. High Energy Phys. 07 (2010) 002.
[44] A. Aguilar and J. Papavassiliou, Phys. Rev. D **77**, 125022 (2008).
[45] A. Cucchieri, T. Mendes, and E. M. Santos, Phys. Rev. Lett. **103**, 141602 (2009).
[46] D. Binosi and A. Quadri, Phys. Rev. D **85**, 121702 (2012).
[47] A. Cucchieri and T. Mendes, arXiv:1204.0216.
[48] A. S. Kronfeld, M. Laursen, G. Schierholz, and U. Wiese, Phys. Lett. B **198**, 516 (1987).
[49] G. Burgio, M. Quandt, and H. Reinhardt, Phys. Rev. D **81**, 074502 (2010); P. Watson and H. Reinhardt, Phys. Rev. D **85**, 025014 (2012).